



## Effects of C/B ratio on glass-forming ability and low-temperature magnetic behavior of FeCoCrMoCBTm metallic glass



Qianqian Wang<sup>a</sup>, Xian Yang<sup>a</sup>, Zhiqiang Cui<sup>a</sup>, Lin Xue<sup>a</sup>, Liliang Shao<sup>a</sup>, Qiang Luo<sup>a</sup>, Baolong Shen<sup>a,b,\*</sup>

<sup>a</sup> School of Materials Science and Engineering, Jiangsu Key Laboratory for Advanced Metallic Materials, Southeast University, Nanjing 211189, China

<sup>b</sup> Institute of Massive Amorphous Metal Science, China University of Mining and Technology, Xuzhou 221116, China

### ARTICLE INFO

#### Article history:

Received 28 August 2020

Received in revised form 1 December 2020

Accepted 3 December 2020

Available online 5 December 2020

#### Keywords:

Fe-based bulk metallic glass

C/B ratio

Spin-glass behavior

Magnetocaloric property

Glass-forming ability

### ABSTRACT

The effects of C/B ratio on the glass-forming ability (GFA) and low-temperature magnetic properties of Fe<sub>42</sub>Co<sub>6</sub>Cr<sub>15</sub>Mo<sub>14</sub>C<sub>x</sub>B<sub>21-x</sub>Tm<sub>2</sub> ( $x = 9, 11, 13, 15$  and  $17$  at%) metallic glasses are studied in this work. The critical diameter of the bulk metallic glasses changes from 2 mm to 12 mm when  $x$  increases from 9 to 15, due to the dense atomic packing and strong liquid behavior. An Fe<sub>42</sub>Co<sub>6</sub>Cr<sub>15</sub>Mo<sub>14</sub>C<sub>15</sub>B<sub>6</sub>Tm<sub>2</sub> amorphous master ingot with a diameter of 16.5 mm is produced via arc melting and furnace cooling. With increasing C/B ratio, the antiferromagnetic interactions between Fe and Cr is decreased, leading to the increasing Curie temperature and activation energy of spin-glass behavior. A stable magnetocaloric transition at a large temperature range is achieved in Fe<sub>42</sub>Co<sub>6</sub>Cr<sub>15</sub>Mo<sub>14</sub>C<sub>15</sub>B<sub>6</sub>Tm<sub>2</sub> glassy ribbon. The fracture strength of the as-cast bulk metallic glasses increases firstly and then decreases with increasing C/B ratio, reaching the highest fracture strength of 4594 MPa when  $x = 15$ .

© 2020 Elsevier B.V. All rights reserved.

### 1. Introduction

Bulk metallic glasses (BMGs) possess unique physical and chemical properties, including high strength, high hardness, large elastic moduli, good corrosion resistance, and high catalytic activity, which make them promising candidate materials for structural and functional applications [1–3]. Among the BMG systems, Fe-based BMGs (Fe-BMGs) have gained the most research attentions due to their excellent soft magnetic properties [4–7]. However, the GFA of Fe-BMGs is worse than most of BMG systems, and their critical diameter is usually below 5 mm. The transition metals-metalloids-rare earth elements (TM-M-RE) BMGs have several advantages in glass-forming, including the significant atomic size mismatch, as well as the negative heat of mixing of TM-M and RE-M pairs [8]. Up to now, the Fe(Co)CrMoCBRE BMGs are the best glass-forming system in Fe-based BMGs [9–11], e.g. the critical diameters of Fe<sub>48</sub>Cr<sub>15</sub>Mo<sub>14</sub>C<sub>15</sub>B<sub>6</sub>Tm<sub>2</sub> is 10 mm [12], of Fe<sub>48</sub>Cr<sub>15</sub>Mo<sub>14</sub>C<sub>15</sub>B<sub>6</sub>Er<sub>2</sub> [13], (Fe<sub>44.3</sub>Cr<sub>5</sub>Co<sub>5</sub>Mo<sub>12.8</sub>Mn<sub>11.2</sub>C<sub>15.8</sub>B<sub>5.9</sub>)<sub>98.5</sub>Y<sub>1.5</sub> and (Fe<sub>44.3</sub>Cr<sub>10</sub>Mo<sub>13.8</sub>Mn<sub>11.2</sub>C<sub>15.8</sub>B<sub>5.9</sub>)<sub>98.5</sub>Y<sub>1.5</sub> BMGs are 12 mm [14], of (Fe<sub>0.8</sub>Co<sub>0.2</sub>)<sub>48</sub>Cr<sub>15</sub>Mo<sub>14</sub>C<sub>15</sub>B<sub>6</sub>Tm<sub>2</sub>, (Fe<sub>0.6</sub>Co<sub>0.4</sub>)<sub>48</sub>Cr<sub>15</sub>Mo<sub>14</sub>C<sub>15</sub>B<sub>6</sub>Tm<sub>2</sub> and Fe<sub>41</sub>Co<sub>7</sub>Cr<sub>15</sub>Mo<sub>14</sub>C<sub>15</sub>B<sub>6</sub>Y<sub>2</sub>

BMGs are 16 mm [15,16]. The concentration ratio of TM and RE elements has been altered and their influence on the GFA has been thoroughly studied in previous works. It has been reported that variation of the C/B ratio can lead to a distinct change of the critical diameter in Fe-based BMGs, for example in FePCB BMG [17]. However, the effect of metalloids C and B concentration on the GFA of these TM-M-RE BMGs is not clear.

In addition, the TM-RE MGs have been reported to show unique low-temperature magnetic properties, including magnetocaloric effect (MCE) and spin-glass (SG) behavior, which can be potentially applied as cryogenic magnetic refrigerant and magnetic storage materials [18,19]. Crystalline magnetic refrigerants usually show giant magnetic entropy change ( $\Delta S_M$ ) due to their first-order magnetic transition. However, their refrigeration capacity (RC) is low because of the narrow full width at half maximum of  $\Delta S_M$  ( $\delta T_{FWHM}$ ), which is a bottle neck problem for the applications in Ericsson cycle [20,21]. In contrast, a combination of large  $|\Delta S_M|$  and RC can be obtained in MGs, which exhibit a second-order magnetic transition. The disordered structure, high thermal stability, tunable transition temperature by alloying and negligible magnetic hysteresis of MGs make them promising magnetic refrigerants. Recently, a series of TM-RE MGs have been reported to show good MCE [22–29], including GdCoAl, GdCoAlFe, GdDyErCoAl, etc. Besides, controllable low-temperature SG behavior, which is an interesting physical phenomenon, has been observed in the TM-RE MGs. The SG behavior

\* Corresponding author at: School of Materials Science and Engineering, Jiangsu Key Laboratory for Advanced Metallic Materials, Southeast University, Nanjing 211189, China.

E-mail address: [blshen@seu.edu.cn](mailto:blshen@seu.edu.cn) (B. Shen).

of GdNiAl MGs disappears when the Ni content is more than 30% [30]. All of the ErDyCoAlRE (RE = Gd, Tb and Tm) high-entropy MGs show distinct SG behavior at cryogenic temperature [24]. However, the effects of metalloids content on the magnetic properties including MCE and SG behavior of this Fe(Co)CrMoCBRE MG system haven't been studied before. In addition, the mechanical performance of the TM-M-RE BMGs is also very important for industrial applications, but the influence of the metalloids on the mechanical properties of this BMG system has not been reported either. Thus, it is of significant importance to elucidate the effects of C/B ratio on the GFA, mechanical property and low-temperature magnetic behavior for the TM-M-RE BMGs.

The electronic structure has been considered as an important factor that determine the formation of BMGs, as well as their magnetic and mechanical properties. Small variations in the bonding of atoms and the hybridization of electron orbitals can lead to distinct changes in GFA. The strong *p-d* hybridization between Al *p* and Co *d* orbitals decrease the density of states (DOS) at Fermi energy level, and promote the formation of string-like aggregates to improve the GFA of ZrCoAl BMGs [31]. Besides, it is well accepted that the mechanical properties of BMG can be tuned by the portion and type of chemical bonds, which are correlated with the electronic structure. For example, the ductility of FeCr-MoPCB BMG is improved by partially replacing B elements that create ionic and covalent bonds with P and C elements that favor metallic cohesion [32]. Furthermore, the magnetic behavior of transition metals is closely related to the hybridization of the 3*d* and 4*s* electron orbitals [33]. Thus, a comprehensive investigation of the TM-M-RE BMGs from the viewpoints of electronic structure can uncover the effects of C/B ratio on the magnetic behavior, glass formation and mechanical property.

In this work, we fabricated Fe<sub>42</sub>Co<sub>6</sub>Cr<sub>15</sub>Mo<sub>14</sub>C<sub>x</sub>B<sub>21-x</sub>Tm<sub>2</sub> (*x* = 9, 11, 13, 15, and 17 at%) glassy ribbons as well as BMGs, and a comprehensive study of their GFA, mechanical and magnetic properties is carried out. The C/B ratio is modified to uncover the effects of metalloids on the GFA, fracture strength, SG behavior and MCE of these BMGs. It is found that the critical diameter increases firstly and then decreases with increasing C/B ratio, and reaches 12 mm when *x* = 15. The highest fracture strength 4594 MPa is achieved in Fe<sub>42</sub>Co<sub>6</sub>Cr<sub>15</sub>Mo<sub>14</sub>C<sub>15</sub>B<sub>6</sub>Tm<sub>2</sub> BMG. The Curie temperature and the activation energy of the SG behavior for the glassy ribbons increase with enhancing C/B ratio. A stable MCE is achieved when *x* = 15. This work successfully clarifies the effects of the metalloids on the glass formation, mechanical property and low-temperature magnetic behavior of FeCoCrMoCBTm MGs.

## 2. Experimental

Master ingots with nominal compositions of Fe<sub>42</sub>Co<sub>6</sub>Cr<sub>15</sub>Mo<sub>14</sub>C<sub>x</sub>B<sub>21-x</sub>Tm<sub>2</sub> (*x* = 9, 11, 13, 15, and 17 at%) were prepared by first induction melting a mixture of pure Fe, Co, Cr, MoC (5.33 wt% C), FeC (5 wt% C) and B, and then arc-melting the obtained ingots with Tm under high purity argon atmosphere. The purities of the raw materials are all higher than 99.9 wt%. The ingots were melted for 5 times to ensure a homogeneous distribution of the elements. The Ribbon and rod samples were prepared by single-roller melt spinning and copper mold suction casting methods, respectively. The amorphous structure of the samples was confirmed by X-ray diffraction (XRD, Bruker D8). Thermal analysis of the samples was carried out by differential scanning calorimetry (DSC, NETZSCH 404 F3). Fracture strength of the as-cast rod samples with a length to diameter ratio of 2:1 were measured using an Instron testing machine at a strain rate of  $2 \times 10^{-1} \text{ s}^{-1}$  under an uniaxial compressive load. AC and DC magnetic properties of the glassy ribbons were measured by a Quantum Design Physical Properties Measurement System (PPMS) and SQUID magnetometer (MPMS), respectively.

The fragility *m* of samples was derived by carrying out DSC analyses of the samples with heating rates ranging from 2 to 50 K/min [34,35]. Fragility parameter *m* was defined by Böhmer and Angell [36]:

$$m = \frac{d \log \eta(T)}{d(T_g/T)} \Big|_{T=T_g} \quad (1)$$

where  $\eta$  is the viscosity. The value of *m* for the amorphous samples could be estimated from the heating rate dependent glass transition temperature  $T_g$ . For glass-forming liquid deviating from Arrhenius behavior, the equilibrium viscosity can be described by the Vogel-Fulcher-Tammann (VFT) equation [37]:

$$\eta = \exp [DT_0/(T - T_0)] \quad (2)$$

The relationship between  $T_g$  and heating rate  $\phi$  can be fitted by an equation with the VFT form:

$$\ln \phi = \ln B - \frac{DT_0}{T_g - T_0} \quad (3)$$

where *B* is a constant associated with a timescale in the glass-forming system, *D* is the fragility parameter which reflects the degree that the liquid system diverges the Arrhenius behavior, and  $T_0$  is a VFT temperature that is usually far below the experimentally measured  $T_g$  within the limit of infinitely slow cooling and heating rates. Subsequently, *m* can be derived based on the following equation:

$$m = \frac{DT_0 T_g}{(T_g - T_0)^2 \ln 10} \quad (4)$$

Electronic structures of the samples were measured by an X-ray photoelectron spectrometer (XPS, ESCALAB 250Xi) equipped with Al K $\alpha$  X-ray source (1486.6 eV). Ribbon samples were cleaned via argon ion sputtering for 500 s before the XPS measurements. Density of samples were measured based on Archimedeian principle.

## 3. Results and discussion

The amorphous nature of the as-cast Fe<sub>42</sub>Co<sub>6</sub>Cr<sub>15</sub>Mo<sub>14</sub>C<sub>x</sub>B<sub>21-x</sub>Tm<sub>2</sub> (*x* = 9, 11, 13, 15 and 17 at%) ribbons were confirmed by XRD before thermal analyses. The thermal properties of the as-cast glassy ribbons are measured by DSC, as shown in Fig. 1, and the values of the thermal parameters for the alloys are summarized in Table 1. As shown in Fig. 1a, upon heating, all of the glassy ribbons exhibit an endothermic glass transition, followed by a supercooled liquid region and then sharp exothermic peaks corresponding to the crystallization process. The values of  $T_g$  and crystallization temperature  $T_x$  shift to lower temperatures with increasing C/B ratio. With increasing C/B ratio, the supercooled liquid region ( $\Delta T_x = T_x - T_g$ ) varies irregularly between 35 and 51 K, and the largest  $\Delta T_x$  (51 K) is obtained when *x* = 11. As shown by the cooling DSC curves in Fig. 1b, the melting temperature  $T_m$  decreases firstly and then increases as the C/B ratio increases, while the liquid temperature  $T_l$  increases monotonously. The alloy with *x* = 9 has the smallest solidification temperature range, which means it is closer to the eutectic point and thus may lead to a better GFA. Based on the above analyses from DSC, it is difficult to evaluate the GFA of the alloys.

To study the effects of C/B ratio on the GFA for Fe<sub>42</sub>Co<sub>6</sub>Cr<sub>15</sub>Mo<sub>14</sub>C<sub>x</sub>B<sub>21-x</sub>Tm<sub>2</sub> (*x* = 9, 11, 13, 15 and 17 at%) BMGs, rod samples are produced via copper mold casting. Fig. 2 shows the XRD patterns of the as-cast rod samples with critical diameters ranging from 2 to 12 mm. All of the patterns exhibit broad diffuse humps, no sharp diffraction peak corresponding to crystalline phase is detected, indicating their amorphous structure. By increasing the C/B ratio, the critical diameter of the alloy increases firstly and then decreases, and reaches the largest value of 12 mm when the C content is 15 at%.

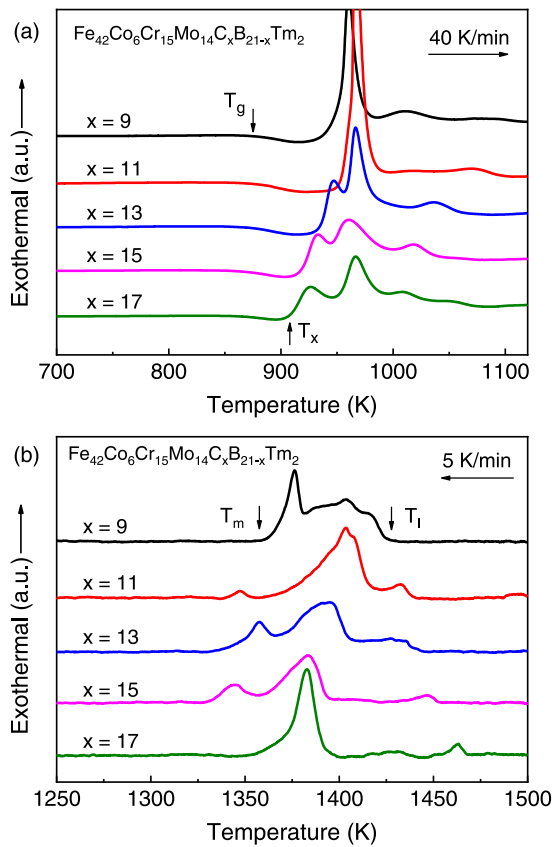


**Fig. 1.** (a) Heating and (b) cooling DSC curves of the as-cast  $\text{Fe}_{42}\text{Co}_6\text{Cr}_{15}\text{Mo}_{14}\text{C}_x\text{B}_{21-x}\text{Tm}_2$  ( $x=9, 11, 13, 15$  and  $17$  at%) glassy ribbons.

Remarkably, as shown in Fig. 3, the  $\text{Fe}_{42}\text{Co}_6\text{Cr}_{15}\text{Mo}_{14}\text{C}_{15}\text{B}_6\text{Tm}_2$  master ingot with a diameter of 16.5 mm is produced via arc melting and furnace cooling, and the whole area of the cross section show metallic luster (the dark areas on the cross sections come from light refraction). The XRD curve of the master ingot is shown in the inset of Fig. 3 and exhibits a diffuse hump, indicating the amorphous nature of this ingot. This further reveals the excellent GFA of this composition. The dimension of the ingot is like a “Frisbee” with the largest thickness of  $\sim 7.5$  mm at the center part, which leads to a large contact surface between ingot and the water-cooled copper mold. Thus, a large cooling rate can be achieved in the ingot, and this explains the amorphous nature of the ingot. Based on the above analysis, modification of C/B ratio obviously influences the glass-forming process in this alloy system. Considering the results from DSC analyses, the variation of GFA is not consistent with  $\Delta T_x$ . Thus, further study about the origin of the largest GFA for BMG with  $x=15$  will be carried out in the later part.

The mechanical properties of the  $\text{Fe}_{42}\text{Co}_6\text{Cr}_{15}\text{Mo}_{14}\text{C}_x\text{B}_{21-x}\text{Tm}_2$  ( $x=9, 11, 13, 15$  and  $17$  at%) BMGs were measured via compressive tests using rod samples with diameters of 2 mm, and length to diameter ratio of 2:1. The compressive stress-strain curves of the BMGs with different C/B ratio are shown in Fig. 4, and the values of

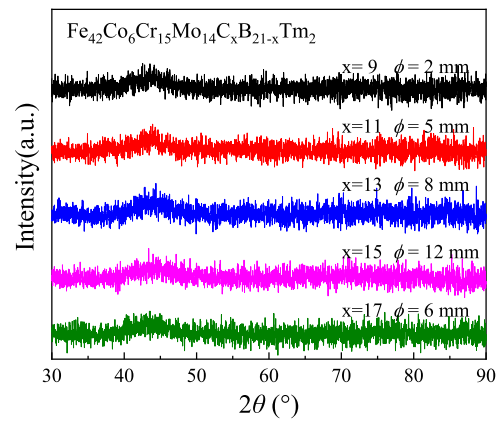


**Fig. 2.** (a) XRD patterns of the as-cast  $\text{Fe}_{42}\text{Co}_6\text{Cr}_{15}\text{Mo}_{14}\text{C}_x\text{B}_{21-x}\text{Tm}_2$  ( $x=9, 11, 13, 15$  and  $17$  at%) rods with critical diameters ranging from 2 to 12 mm.

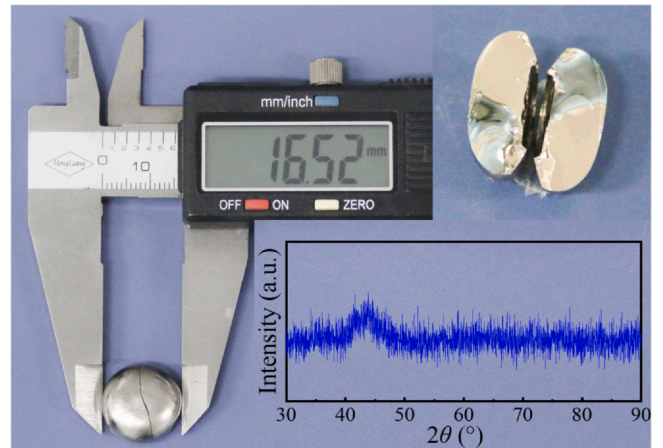


**Fig. 3.** (c) The photos of the  $\text{Fe}_{42}\text{Co}_6\text{Cr}_{15}\text{Mo}_{14}\text{C}_{15}\text{B}_6\text{Tm}_2$  ingot and its cross section. The XRD pattern of the ingot is shown in the inset.

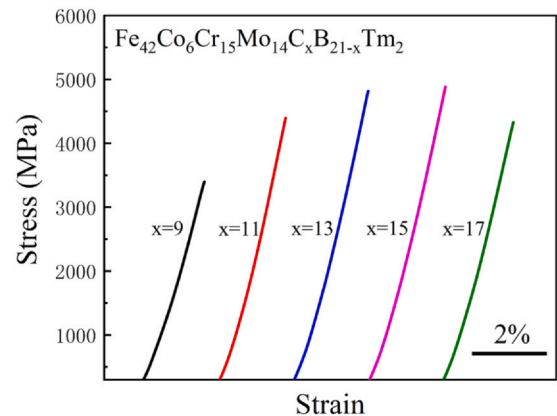


**Fig. 4.** Compressive stress-strain curves at room temperature for  $\text{Fe}_{42}\text{Co}_6\text{Cr}_{15}\text{Mo}_{14}\text{C}_x\text{B}_{21-x}\text{Tm}_2$  ( $x=9, 11, 13, 15$  and  $17$  at%) BMGs.

**Table 1**

Critical diameter ( $D_c$ ), glass transition temperature ( $T_g$ ), crystallization temperature ( $T_x$ ), melting temperature ( $T_m$ ), liquid temperature ( $T_l$ ), supercooled liquid region ( $\Delta T_x$ ), fragility ( $m$ ), spin-frozen temperature ( $T_f$ ), Curie temperature ( $T_C$ ) and compressive fracture strength ( $\sigma_f$ ) of  $\text{Fe}_{42}\text{Co}_6\text{Cr}_{15}\text{Mo}_{14}\text{C}_x\text{B}_{21-x}\text{Tm}_2$  ( $x=9, 11, 13, 15$  and  $17$  at%) metallic glasses.

Alloy	$D_c$ (mm)	$T_g$ (K)	$T_x$ (K)	$T_m$ (K)	$T_l$ (K)	$\Delta T_x$ (K)	$\rho$ (g/cm <sup>3</sup> )	$m$	$T_f$ (K)	$T_C$ (K)	$\sigma_f$ (MPa)
$x=9$	2	876	925	1366	1427	49	7.81	55	8	18	3500
$x=11$	5	872	923	1339	1440	51	7.83	50	8	19	3738
$x=13$	8	871	908	1328	1444	37	8.06	47	8	20	4295
$x=15$	12	850	893	1327	1452	43	8.47	41	8	23	4594
$x=17$	6	845	880	1354	1468	35	7.88	80	8	25	4076

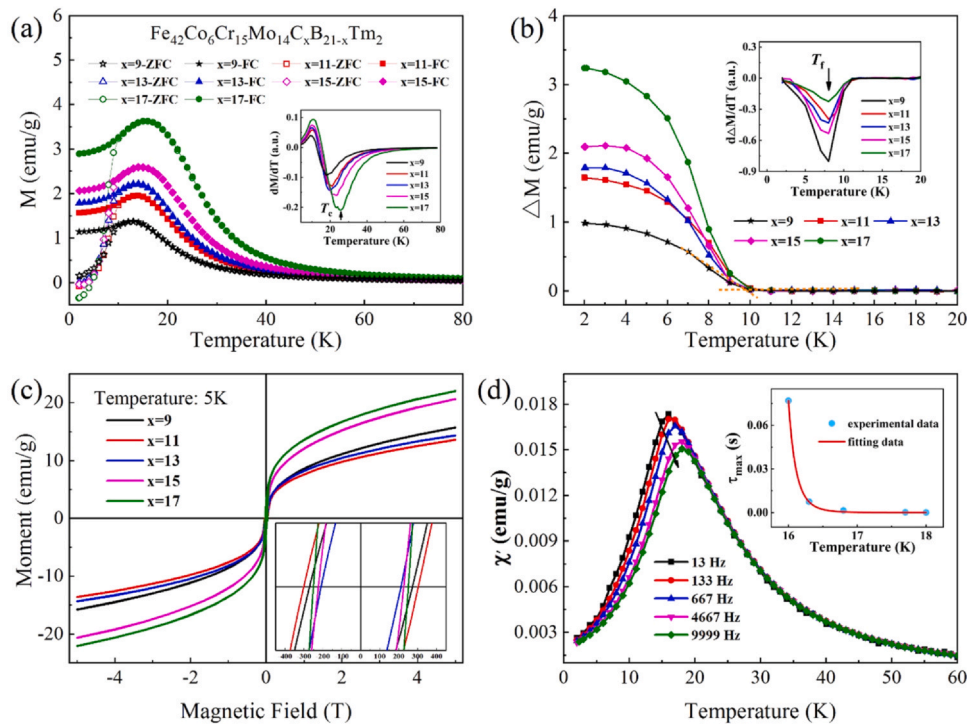


**Fig. 5.** SG behavior analyses of the as-cast  $\text{Fe}_{42}\text{Co}_6\text{Cr}_{15}\text{Mo}_{14}\text{C}_x\text{B}_{21-x}\text{Tm}_2$  ( $x = 9, 11, 13, 15$  and  $17$  at%) glassy ribbons (a) ZFC and FC magnetization curves under a magnetic field of  $0.02$  T, and the inset shows differential curves. (b) The difference value between FC and ZFC magnetization, the inset shows the differential curves. (c) Hysteresis loops, and the inset shows the magnification around zero applied field. (d) AC susceptibility curves at different frequencies, and the inset shows the relaxation time  $\tau_{\text{max}}$  versus temperature and the solid line is fitting curve.

fracture strength are listed in Table 1. All of the samples show brittle fracture, as no plastic deformation is observed on the stress-strain curves. When  $x$  increases from 9 to 15, the fracture strength keeps rising, but drops with further increase of C. The BMG with  $x = 15$  exhibits highest fracture strength of  $4594$  MPa. The origin of the variation of the fracture strength with increasing C content will be explained via the electronic structure analyses.

The combination of TM and RE elements usually lead to interesting magnetic behavior, thus the SG behavior and MCE of the  $\text{Fe}_{42}\text{Co}_6\text{Cr}_{15}\text{Mo}_{14}\text{C}_x\text{B}_{21-x}\text{Tm}_2$  ( $x = 9, 11, 13, 15$  and  $17$  at%) glassy ribbons are analyzed. The SG behavior of glassy ribbons are investigated by measuring the magnetic response of the samples at different temperatures and applied fields. Fig. 5a shows the temperature dependent field cooling (FC) and zero field cooling (ZFC) magnetization curves for  $\text{Fe}_{42}\text{Co}_6\text{Cr}_{15}\text{Mo}_{14}\text{C}_x\text{B}_{21-x}\text{Tm}_2$  ( $x = 9, 11, 13, 15$  and  $17$  at%) glassy ribbons. These ribbons exhibit ferromagnetic characteristics below  $30$  K. When the temperature is higher than  $30$  K, the magnetization of the ribbons decreases and approaches to zero, indicating a ferromagnetic to paramagnetic phase transition. As the C/B ratio increases, both the magnetization and the transition temperature increase substantially. For all of the MGs, obvious divergence between FC and ZFC branches occurs around  $10$  K, showing a typical SG-like behavior. Fig. 5b shows the difference between FC and ZFC magnetization for the alloys, which also increases with the rising C/B ratio. The Curie temperatures ( $T_C$ ) and the spin freezing temperatures ( $T_f$ ), which were defined as the temperatures corresponding to the minimum of  $dM/dT$  and  $d\Delta M/dT$ , are shown in the insets of Fig. 5a and b, respectively. The values of  $T_C$  and  $T_f$  are calculated and listed in Table 1. As the C/B ratio increases,  $T_C$  increases gradually while the  $T_f$  keeps constant. This indicates that the increase of the C/B ratio promotes the ferromagnetic exchange interaction, but has almost no effect on the random magnetic anisotropy below  $T_C$  of this alloy system. In this Fe-based metallic glass system, the long-range ferromagnetic order was broken by the large random

magnetic anisotropy induced by the rare earth Tm element. The spins are oriented along their anisotropy axes under local anisotropy field at low temperature, which causes the formation of complex ground states with a random orientation of magnetic moments and magnetic irreversibility.

Hysteresis loops under a magnetic field of  $5$  T at  $5$  K were measured for  $\text{Fe}_{42}\text{Co}_6\text{Cr}_{15}\text{Mo}_{14}\text{C}_x\text{B}_{21-x}\text{Tm}_2$  ( $x = 9, 11, 13, 15$  and  $17$  at%) glassy ribbons as shown in Fig. 5c. All of the ribbons exhibit overlapping loops and soft magnetic characteristics at low temperature. As the applied field increases, the samples are magnetized fast and tend to be saturated. As shown by the enlarged hysteresis loops around  $0$  T, the glassy ribbons exhibit very low coercivity of  $0.02$ – $0.03$  T, which results from the random magnetic anisotropy caused by the interaction between the  $3d$  electrons in transition metals and  $4f$  electrons in the Tm element.

To further investigate the SG behavior in these MGs, the critical dynamics of the SG transition for the representative  $\text{Fe}_{42}\text{Co}_6\text{Cr}_{15}\text{Mo}_{14}\text{C}_{15}\text{B}_6\text{Tm}_2$  glassy ribbon is studied. AC susceptibility at different frequencies for  $\text{Fe}_{42}\text{Co}_6\text{Cr}_{15}\text{Mo}_{14}\text{C}_{15}\text{B}_6\text{Tm}_2$  glassy ribbon were measured and plotted in Fig. 5d. Sharp peaks can be observed on the susceptibility curves for all of the frequencies. The peak positions shift to higher temperatures and decrease with increasing frequency, exhibiting a typical SG-like behavior. For a critical slowing down dynamics, the correlation length diverges at the transition temperature and the relaxation time  $\tau_{\text{max}}$  obeys the following law [38]:

$$\tau_{\text{max}} = \tau_0 \times T_f/T_s - 1^{2\nu} \quad (5)$$

where  $T_s$  and  $z\nu$  are the ideal freezing temperature and a critical exponent, respectively,  $\tau_0$  is related to the relaxation time of individual atomic magnetic moment. For antitype spin-glasses,  $\tau_0$  is about  $10^{-10}$ – $10^{-13}$  s and  $z\nu$  is reported to be  $4$ – $13$  [38]. The experimental data were well fitted with Eq. 5, as shown in the inset of

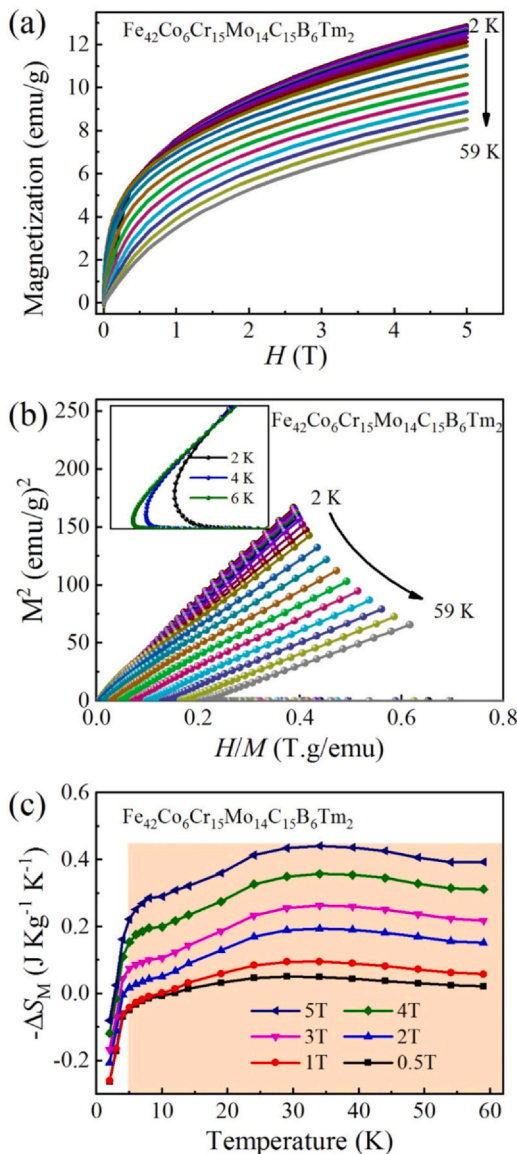


**Fig. 6.** (a) The isothermal magnetization curves of Fe<sub>42</sub>Co<sub>6</sub>Cr<sub>15</sub>Mo<sub>14</sub>C<sub>15</sub>B<sub>6</sub>Tm<sub>2</sub> glassy ribbon from 2 to 59 K, (b) the corresponding Arrott plots and (c) the  $-\Delta S_M$  versus temperature at various magnetic field. The inset of (b) shows the Arrott plots at 2, 4 and 6 K.

Fig. 5d. The fitting results are:  $\tau_0 = \sim 10^{-11}$  s,  $T_s = 15.2$  K and  $z\nu = 7.1$ . Both the  $\tau_0$  and  $z\nu$  values locate in the range of conventional SG systems, demonstrating a critical divergence and the existence of a SG-like behavior in this BMG.

The MCE of the Fe<sub>42</sub>Co<sub>6</sub>Cr<sub>15</sub>Mo<sub>14</sub>C<sub>15</sub>B<sub>6</sub>Tm<sub>2</sub> glassy ribbon, which has the largest GFA, is studied by measuring the isothermal magnetization at temperatures ranging from 2 to 59 K. As shown in Fig. 6a, the magnetization of the sample rises and then approaches to saturation with increasing applied magnetic field up to 5 T. Besides, the susceptibility and magnetization decrease gradually as the temperature rises, confirming the ferromagnetic to paramagnetic transition. Fig. 6b shows the corresponding Arrott plots, and the inset shows the magnified plots at 2, 4 and 6 K. According to Banerjee criterion, the magnetic transition in Fe<sub>42</sub>Co<sub>6</sub>Cr<sub>15</sub>Mo<sub>14</sub>C<sub>15</sub>B<sub>6</sub>Tm<sub>2</sub> glassy ribbon is a second-order phase transition due to the positive slope of Arrott plots [39], which indicates a low hysteresis during the transition process. The intersection at low temperatures is attributed to the SG-like behavior. As one of the main parameters to characterize the MCE, the  $\Delta S_M$  can be derived from the isothermal

magnetization curves by integrating the Maxwell relation over the magnetic field [38]:

$$\Delta S_M(T, H) = S_M(T, H) - S_M(T, 0) = \int_{H_0}^{H_{\max}} \left( \frac{\partial M}{\partial T} \right) dH \quad (6)$$

where  $H_{\max}$  represents the maximum value of the magnetic field, and  $H_0$  is 0 T in this work. Generally, the  $-\Delta S_M$  increases with the increasing applied magnetic field, because the magnetic order changes substantially at high applied magnetic field. Fig. 6c exhibits the temperature dependence of  $-\Delta S_M$  under different magnetic fields for Fe<sub>42</sub>Co<sub>6</sub>Cr<sub>15</sub>Mo<sub>14</sub>C<sub>15</sub>B<sub>6</sub>Tm<sub>2</sub> glassy ribbon. Under an applied magnetic field of 5 T, the maximum of magnetic entropy change ( $-\Delta S_M^{\max}$ ) is 0.44 J kg<sup>-1</sup> K<sup>-1</sup>. The RC can be estimated using Gschneidner method as shown in Eq. 7 [40]:

$$RC = -\Delta S_M^{\max} \times \delta T_{FWHM} \quad (7)$$

Under an applied magnetic field of 5 T with the temperature range up to 59 K, the RC of Fe<sub>42</sub>Co<sub>6</sub>Cr<sub>15</sub>Mo<sub>14</sub>C<sub>15</sub>B<sub>6</sub>Tm<sub>2</sub> glassy ribbon is 23.8 J kg<sup>-1</sup>. The  $-\Delta S_M^{\max}$  and RC values are not very prominent compared with other amorphous magnetic refrigerants. However, within the temperature range from 5 to 59 K, this glassy ribbon exhibits a constant  $-\Delta S_M$  value, demonstrating a table-like MCE, as shown by the orange shading in Fig. 6c. This guarantees a stable magnetocaloric transition process and a large working temperature range of this MG, which is favorable to the application in the Ericsson cycle.

By modification of C/B ratio, the GFA, mechanical properties and low-temperature magnetic behavior of FeCoCrMoCBTm MGs is optimized. An Fe<sub>42</sub>Co<sub>6</sub>Cr<sub>15</sub>Mo<sub>14</sub>C<sub>15</sub>B<sub>6</sub>Tm<sub>2</sub> MG with a large critical diameter of 12 mm, high fracture strength of 4594 MPa, distinct SG behavior and stable MCE is fabricated. In order to elucidate the relationship between the modified C/B ratio and varied GFA, mechanical performance and magnetic behavior, the fragility of melting liquids and electronic structure of the as-cast MGs are studied comprehensively.

The properties of the supercooled liquids are investigated by carrying out DSC analyses with different heating rates for Fe<sub>42</sub>Co<sub>6</sub>Cr<sub>15</sub>Mo<sub>14</sub>C<sub>x</sub>B<sub>21-x</sub>Tm<sub>2</sub> ( $x = 9, 11, 13, 15$  and 17 at%) glassy ribbons. The representative DSC curves of Fe<sub>42</sub>Co<sub>6</sub>Cr<sub>15</sub>Mo<sub>14</sub>C<sub>11</sub>B<sub>10</sub>Tm<sub>2</sub> glassy ribbon with heating rates ranging from 2 to 50 K/min are shown in Fig. 7a. By increasing the heating rate, the glass transition and crystallization phenomenon become more distinct, and both  $T_g$  and  $T_x$  shift to higher temperatures. To better characterize the liquid behavior of the BMGs, the fragility parameter  $m$  was calculated. The  $m$  was reported to have inherent relations with bonding and viscosity behaviors of glass-forming liquids, hence the GFA of BMGs can be explained based on the  $m$  value. The smaller the  $m$  value is, the "stronger" the liquid is, and usually corresponding to a larger GFA [41,42]. Fig. 7b shows the VFT fitting plots of the thermal properties for Fe<sub>42</sub>Co<sub>6</sub>Cr<sub>15</sub>Mo<sub>14</sub>C<sub>x</sub>B<sub>21-x</sub>Tm<sub>2</sub> ( $x = 9, 11, 13, 15$  and 17 at%) glassy ribbons, and the estimated values of  $m$  are listed in Table 1. When the C/B ratio increases, the value of  $m$  decreases firstly and then increases, exhibiting a minimum of 41 at  $x = 15$ . This indicates that the Fe<sub>42</sub>Co<sub>6</sub>Cr<sub>15</sub>Mo<sub>14</sub>C<sub>15</sub>B<sub>6</sub>Tm<sub>2</sub> liquid is strong. In strong liquids, only a small amount of local atomic rearrangements occur during glass transition, while a collective rearrangements of atom groups predominant in fragile liquids. Thus, the Fe<sub>42</sub>Co<sub>6</sub>Cr<sub>15</sub>Mo<sub>14</sub>C<sub>15</sub>B<sub>6</sub>Tm<sub>2</sub> BMG exhibits smaller changes in the structure and heat capacity with changing temperature in the glass transition region, and possesses more sluggish dynamics and crystallization kinetics, which make it a better glass former.

As GFA of BMGs is affected by their electronic structure, the effects of C/B ratio on the bonding states of the Fe<sub>42</sub>Co<sub>6</sub>Cr<sub>15</sub>Mo<sub>14</sub>C<sub>x</sub>B<sub>21-x</sub>Tm<sub>2</sub> ( $x = 9, 11, 13, 15$  and 17 at%) MGs are analyzed by XPS. No obvious change of the binding energies is detected for Fe 2p, Co 2p or

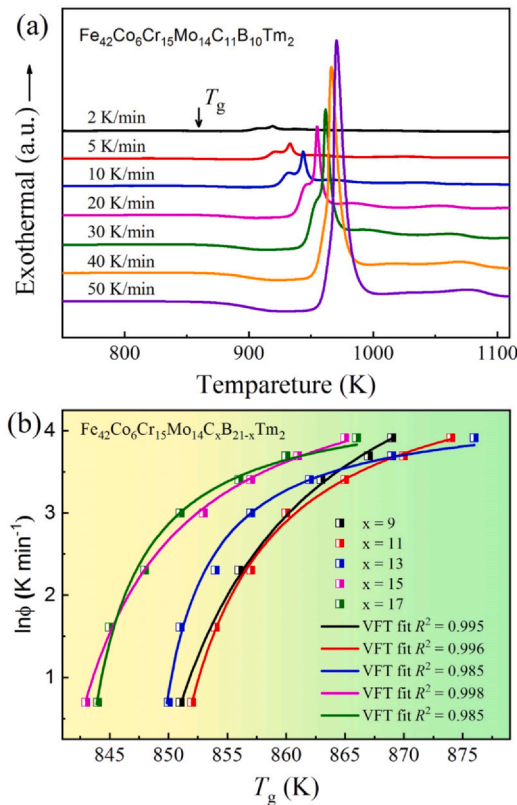


**Fig. 7.** (a) DSC curves of  $\text{Fe}_{42}\text{Co}_6\text{Cr}_{15}\text{Mo}_{14}\text{C}_{11}\text{B}_{10}\text{TM}_2$  glassy ribbons with different heating rates and (b) The heating rate dependent of  $T_g$  for  $\text{Fe}_{42}\text{Co}_6\text{Cr}_{15}\text{Mo}_{14}\text{C}_x\text{B}_{21-x}\text{TM}_2$  ( $x = 9, 11, 13, 15$  and  $17$  at%) glassy ribbons, and solid lines are VFT fittings.

Mo 3d. The B 1s, C 1s and Cr  $2p_{3/2}$  core level spectra obtained for the samples are shown in Fig. 8a, b and c, respectively. The magnified images of the peaks are shown in the insets of corresponding figures. With increasing C/B ratio, the core-level peaks of B 1s and C 1s shift to lower binding energies firstly and then to higher values, reaching the minimum value at  $x = 15$ . The variation in binding energies is consistent with the variation of the GFA in this Fe-based BMG system. Although the relative variations of the binding energies are less than 0.1 eV, the small change in the electronic structure can significantly affect the GFA of the BMGs [43]. The electron orbital hybridization of the transition metals and metalloids results in the change of the binding energies of C 1s and B 1s. The smallest binding energies of the metalloids in the alloy with  $x = 15$  may come from the densest atomic packing structure. To verify this proposal, the density  $\rho$  of the BMGs were measured and shown in Table 1. It is true that the density of the samples increases when  $x$  increases from 9 to 15, and then decreases with further increasing C/B ratio. The dense atomic packing impedes the rearrangement of atoms to form crystals, thus leads to the large GFA of  $\text{Fe}_{42}\text{Co}_6\text{Cr}_{15}\text{Mo}_{14}\text{C}_{15}\text{B}_6\text{TM}_2$  BMG.

Besides, BMGs with denser atomic packing usually has higher fracture strength [44]. The BMGs with smaller atomic spacing have less space available for the atoms to move around their nearest neighbor without energy change. A larger driven force is needed for the movement of atoms, thus the stress value before yielding is increased. As a result, the  $\text{Fe}_{42}\text{Co}_6\text{Cr}_{15}\text{Mo}_{14}\text{C}_{15}\text{B}_6\text{TM}_2$  BMG has the highest strength. The low-temperature magnetic behavior of the Fe-based glassy ribbons is related to the change of electronic structure with C/B ratio variation. As shown in Fig. 5, the peak temperatures of ZFC and FC magnetization, as well as the decline rate of the FC magnetization, increases obviously with increasing C/B ratio. This indicates the activation energy for SG behavior is improved in the glassy ribbon with higher C content. Also, the  $T_C$  increases with

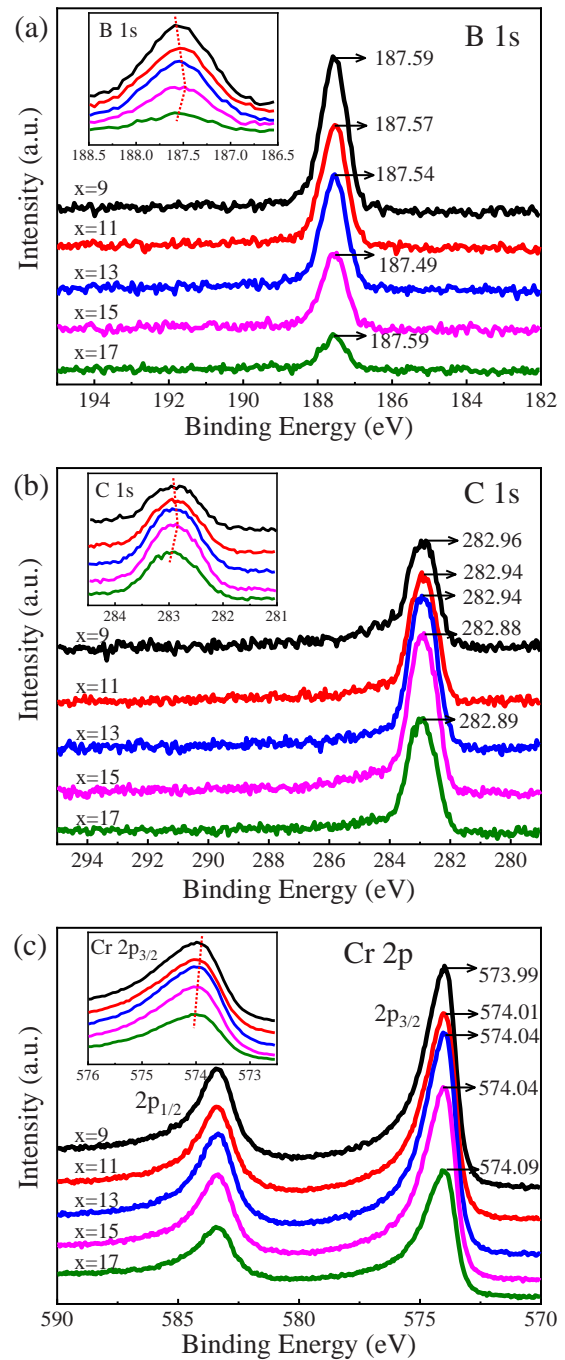


**Fig. 8.** The binding energies of (a) B 1s, (b) C 1s and (c) Cr 2p for the as-cast  $\text{Fe}_{42}\text{Co}_6\text{Cr}_{15}\text{Mo}_{14}\text{C}_x\text{B}_{21-x}\text{TM}_2$  ( $x = 9, 11, 13, 15$  and  $17$  at%) glassy ribbons. The insets are the magnifications at peak positions.

enhancing C/B ratio. As shown in Fig. 7c, the binding energy of Cr  $2p_{3/2}$  increases linearly with higher C content, due to the occupation of C atoms around Cr atoms. The antiferromagnetic interactions between Fe and Cr is then reduced. Besides, as C atoms can provide more electrons to Fe than B atoms, the distribution of magnetic interactions can be affected. This explains the improved  $T_C$  and activation energy of SG behavior with increasing C/B ratio.

#### 4. Conclusions

In this work, the effects of C/B ratio on the GFA, fracture strength and low-temperature magnetic behavior of  $\text{Fe}_{42}\text{Co}_6\text{Cr}_{15}\text{Mo}_{14}\text{C}_x\text{B}_{21-x}$

$x\text{TM}_2$  ( $x = 9, 11, 13, 15$  and  $17$  at%) MGs are systematically studied. An  $\text{Fe}_{42}\text{Co}_6\text{Cr}_{15}\text{Mo}_{14}\text{C}_{15}\text{B}_6\text{TM}_2$  BMG with critical diameter of 12 mm, fracture strength of 4594 MPa, distinct spin-glass behavior and stable magnetocaloric transition at a large temperature range is fabricated. The electronic structure and liquid behavior analyses of the BMGs reveal that the large GFA of this BMG is related to its dense atomic packing and strong liquid behavior. The high fracture strength of this alloy also results from the dense atomic packing, while the distinct spin-glass behavior is attributed to the large random magnetic anisotropy.

### CRedit authorship contribution statement

**Qianqian Wang:** Conceptualization, Investigation, Writing - original draft. **Xian Yang:** Investigation, Methodology. **Zhiqiang Cui:** Investigation, Methodology. **Lin Xue:** Conceptualization, Writing - original draft. **Liliang Shao:** Conceptualization, Writing - review & editing. **Qiang Luo:** Conceptualization. **Baolong Shen:** Conceptualization, Supervision, Project administration, Funding acquisition, Writing - review & editing.

### Declaration of Competing Interest

The authors declare that they have no known competing financial interests or personal relationships that could have appeared to influence the work reported in this paper.

### Acknowledgments

This work was supported by the National Natural Science Foundation of China (Grant No. 51631003), the Natural Science Foundation of Jiangsu Province of China (Grant No. BK20191269), and the Fundamental Research Funds for the Central Universities (Grant No. 2242019k1G005).

### References

- [1] W.H. Wang, The elastic properties, elastic models and elastic perspectives of metallic glasses, *Prog. Mater. Sci.* 57 (2012) 487–656.
- [2] D.D. Xu, B.L. Zhou, Q.Q. Wang, J. Zhou, W.M. Yang, C.C. Yuan, L. Xue, X.D. Fan, L.Q. Ma, B.L. Shen, Effects of Cr addition on thermal stability, soft magnetic properties and corrosion resistance of FeSiB amorphous alloys, *Corros. Sci.* 138 (2018) 20–27.
- [3] Y.C. Hu, Y.Z. Wang, R. Su, C.R. Cao, F. Li, C.W. Sun, Y. Yang, P.F. Guan, D.W. Ding, Z.L. Wang, W.H. Wang, A highly efficient and self-stabilizing metallic-glass catalyst for electrochemical hydrogen generation, *Adv. Mater.* 28 (2016) 10293–10297.
- [4] H.X. Li, Z.C. Lu, S.L. Wang, Y. Wu, Z.P. Lu, Fe-based bulk metallic glasses: glass formation, fabrication, properties and applications, *Prog. Mater. Sci.* 103 (2019) 235–318.
- [5] W.M. Yang, H.S. Liu, Y.C. Zhao, A. Inoue, K.M. Jiang, J.T. Huo, H.B. Ling, Q. Li, B.L. Shen, Mechanical properties and structural features of novel Fe-based bulk metallic glasses with unprecedented plasticity, *Sci. Rep.* 4 (2014) 6233.
- [6] A. Inoue, B.L. Shen, C.T. Chang, Super-high strength of over 4000 MPa for Fe-based bulk glassy alloys in  $[(\text{Fe}_{1-x}\text{Co}_x)_{0.75}\text{B}_{0.2}\text{Si}_{0.05}]_{96}\text{Nb}_4$  system, *Acta Mater.* 52 (2004) 4093–4099.
- [7] C. Liu, Q. Li, J.T. Huo, L. Xie, W.M. Yang, C.T. Chang, Y.F. Sun, Effect of preparation cooling rate on magnetocaloric effect of  $\text{Fe}_{80}\text{P}_{13}\text{C}_7$  amorphous alloy, *J. Magn. Magn. Mater.* 475 (2019) 249–256.
- [8] A. Takeuchi, A. Inoue, Classification of bulk metallic glasses by atomic size difference, heat of mixing and period of constituent elements and its application to characterization of the main alloying element, *Mater. Trans.* 46 (2005) 2817–2829.
- [9] S.J. Pang, T. Zhang, K. Asami, A. Inoue, Bulk glassy Fe-Cr-Mo-C-B alloys with high corrosion resistance, *Corros. Sci.* 44 (2002) 1847–1856.
- [10] S.J. Pang, T. Zhang, K. Asami, A. Inoue, Synthesis of Fe-Cr-Mo-C-B-P bulk metallic glasses with high corrosion resistance, *Acta Mater.* 50 (2002) 489–497.
- [11] V. Ponnambalam, S.J. Poon, G.J. Shiflet, V.M. Keppens, R. Taylor, G. Petculescu, Synthesis of iron-based bulk metallic glasses as nonferromagnetic amorphous steel alloys, *Appl. Phys. Lett.* 83 (2003) 1131–1133.
- [12] K. Amiya, A. Inoue, Fe-(Cr,Mo)-(C,B)-Tm bulk metallic glasses with high strength and high glass-forming ability, *Mater. Trans.* 47 (2006) 1615–1618.
- [13] V. Ponnambalam, S.J. Poon, G.J. Shiflet, Fe-based bulk metallic glasses with diameter thickness larger than one centimeter, *J. Mater. Res.* 19 (2004) 1320–1323.
- [14] Z.P. Lu, C.T. Liu, J.R. Thompson, W.D. Porter, Structural amorphous steels, *Phys. Rev. Lett.* 92 (2004) 245503.
- [15] K. Amiya, A. Inoue, Fe-(Cr, Mo)-(C, B)-Tm bulk metallic glasses with high strength and high glass-forming ability, *Rev. Adv. Mater. Sci.* 18 (2008) 27–29.
- [16] J. Shen, Q. Chen, J. Sun, H. Fan, G. Wang, Exceptionally high glass-forming ability of an FeCoCrMoCBy alloy, *Appl. Phys. Lett.* 86 (2005) 151907.
- [17] M.D. Demetriou, G. Kaltenboeck, J.Y. Suh, G. Garrett, M. Floyd, C. Creadson, D.C. Hofmann, H. Kozachkov, A. Wiest, J.P. Schramm, W.L. Johnson, Glassy steel optimized for glass-forming ability and toughness, *Appl. Phys. Lett.* 95 (2009) 041907.
- [18] H.X. Shen, L. Luo, Y. Bao, H.B.C. Yin, S.D. Jiang, L.Y. Zhang, Y.J. Huang, S.J. Feng, D.W. Xing, J.S. Liu, Z. Li, Y.F. Liu, J.F. Sun, M.H. Phan, New DyHoCo medium entropy amorphous microwires of large magnetic entropy change, *J. Alloy. Compd.* 837 (2020) 155431.
- [19] Y.M. Wang, D. Guo, B.B. Wu, S.H. Geng, Y.K. Zhang, Magnetocaloric effect and refrigeration performance in  $\text{RE}_{60}\text{Co}_{20}\text{Ni}_{20}$  (RE = Ho and Er) amorphous ribbons, *J. Magn. Magn. Mater.* 498 (2020) 166179.
- [20] V.K. Pecharsky, K.A. Gschneidner, Magnetocaloric effect and magnetic refrigeration, *J. Magn. Magn. Mater.* 200 (1999) 44–56.
- [21] K.A. Gschneidner, V.K. Pecharsky, A.O. Tsokol, Recent developments in magnetocaloric materials, *Rep. Prog. Phys.* 68 (2005) 1479–1539.
- [22] Q. Luo, J. Shen, Reentrant spin glass ordering in an Fe-based bulk metallic glass, *J. Appl. Phys.* 117 (2015) 053909.
- [23] L. Xue, J. Li, W.M. Yang, C.C. Yuan, B.L. Shen, Effect of Fe substitution on magnetocaloric effects and glass-forming ability in Gd-based metallic glasses, *Intermetallics* 93 (2018) 67–71.
- [24] J. Li, L. Xue, W.M. Yang, C.C. Yuan, J.T. Huo, B.L. Shen, Distinct spin glass behavior and excellent magnetocaloric effect in  $\text{Er}_{20}\text{Dy}_{20}\text{Co}_{20}\text{Al}_{20}\text{RE}_{20}$  (RE = Gd, Tb and Tm) high-entropy bulk metallic glasses, *Intermetallics* 96 (2018) 90–93.
- [25] Q. Luo, X.D. Zhang, B.L. Shen, Tunability of correlated magnetocaloric effect and magnetoresistance by Ar ion irradiation in a Gd-based nanocrystalline/amorphous alloy, *J. Alloy. Compd.* 788 (2019) 283–288.
- [26] L. Xue, L.L. Shao, Q. Luo, B.L. Shen,  $\text{Gd}_{25}\text{RE}_{25}\text{Co}_{25}\text{Al}_{25}$  (RE = Tb, Dy and Ho) high-entropy glassy alloys with distinct spin-glass behavior and good magnetocaloric effect, *J. Alloy. Compd.* 790 (2019) 633–639.
- [27] L. Xue, Q. Luo, L.L. Shao, B.L. Shen, Magnetocaloric difference between ribbon and bulk shape of Gd-based metallic glasses, *J. Magn. Magn. Mater.* 497 (2020) 166015.
- [28] L. Shao, L. Xue, Q. Luo, Q. Wang, B. Shen, The role of Co/Al ratio in glass-forming GdCoAl magnetocaloric metallic glasses, *Materialia* 7 (2019) 100419.
- [29] C.M. Pang, L. Chen, H. Xu, W. Guo, Z.W. Lv, J.T. Huo, M.J. Cai, B.L. Shen, X.L. Wang, C.C. Yuan, Effect of Dy, Ho, and Er substitution on the magnetocaloric properties of Gd-Co-Al-Y high entropy bulk metallic glasses, *J. Alloy. Compd.* 827 (2020) 154101.
- [30] F. Yuan, J. Du, B. Shen, Controllable spin-glass behavior and large magnetocaloric effect in Gd-Ni-Al bulk metallic glasses, *Appl. Phys. Lett.* 101 (2012) 032405.
- [31] C.C. Yuan, F. Yang, X.K. Xi, C.L. Shi, D. Holland-Moritz, M.Z. Li, F. Hu, B.L. Shen, X.L. Wang, A. Meyer, W.H. Wang, Impact of hybridization on metallic-glass formation and design, *Mater. Today* 32 (2020) 26–34.
- [32] X.J. Gu, S.J. Poon, G.J. Shiflet, M. Widom, Ductility improvement of amorphous steels: Roles of shear modulus and electronic structure, *Acta Mater.* 56 (2008) 88–94.
- [33] W.M. Yang, Q.Q. Wang, W.Y. Li, L. Xue, H.S. Liu, J. Zhou, J.Y. Mo, B.L. Shen, A novel thermal-tuning Fe-based amorphous alloy for automatically recycled methylene blue degradation, *Mater. Des.* 161 (2019) 136–146.
- [34] R. Böhmer, K.L. Ngai, C.A. Angell, D.J. Plazek, Nonexponential relaxations in strong and fragile glass formers, *J. Chem. Phys.* 99 (1993) 4201–4209.
- [35] C.A. Angell, Formation of glasses from liquids and biopolymers, *Science* 267 (1995) 1924–1935.
- [36] R. Böhmer, C.A. Angell, Correlations of the nonexponentiality and state dependence of mechanical relaxations with bond connectivity in Ge-As-Se supercooled liquids, *Phys. Rev. B* 45 (1992) 10091–10094.
- [37] G.S. Fulcher, Analysis of recent measurements of the viscosity of glasses, *J. Am. Ceram. Soc.* 8 (1925) 339–355.
- [38] K. Binder, A.P. Young, Spin glasses: experimental facts, theoretical concepts, and open questions, *Rev. Mod. Phys.* 58 (1986) 801–976.
- [39] J. Fan, L. Ling, B. Hong, L. Zhang, L. Pi, Y. Zhang, Critical properties of the perovskite manganite  $\text{La}_{0.1}\text{Nd}_{0.6}\text{Sr}_{0.3}\text{MnO}_3$ , *Phys. Rev. B* 81 (2010) 144426.
- [40] K.A. Gschneidner, V.K. Pecharsky, Magnetocaloric materials, *Annu. Rev. Mater. Sci.* 30 (2000) 387–429.
- [41] E.S. Park, J.H. Na, D.H. Kim, Correlation between fragility and glass-forming ability/plasticity in metallic glass-forming alloys, *Appl. Phys. Lett.* 91 (2007) 031907.
- [42] J.C. Bendert, A.K. Gangopadhyay, N.A. Mauro, K.F. Kelton, Volume expansion measurements in metallic liquids and their relation to fragility and glass forming ability: an energy landscape interpretation, *Phys. Rev. Lett.* 109 (2012) 185901.
- [43] J.W. Li, D. Estévez, K.M. Jiang, W.M. Yang, Q.K. Man, C.T. Chang, X.M. Wang, Electronic-structure origin of the glass-forming ability and magnetic properties in Fe-RE-B-Nb bulk metallic glasses, *J. Alloy. Compd.* 617 (2014) 332–336.
- [44] Q.Q. Wang, J. Zhou, Q.S. Zeng, G.L. Zhang, K.B. Yin, T. Liang, W.M. Yang, M. Stoica, L.T. Sun, B.L. Shen, Ductile Co-based bulk metallic glass with superhigh strength and excellent soft magnetic properties induced by modulation of structural heterogeneity, *Materialia* 9 (2020) 100561.